# Characterization of Dopant Diffusion within Semiconducting Polymer and Small-Molecule Films Using Infrared-Active Vibrational Modes and Attenuated Total Reflectance Infrared Spectroscopy

Ashok J. Maliakal*

LGS Innovations, 15 Vreeland Road, Florham Park, New Jersey 07932, United States

ABSTRACT: Understanding dopant diffusion within organic and polymeric semiconductors is of great importance toward the development of organic photovoltaic and electronic devices, many of which require layered structures with controlled doping profiles (e.g., p−n and p−i−n structures). The current paper demonstrates a new method to determine the diffusion and permeability coefficients for dopant diffusion within polymeric and small-molecule organic semiconductors using attenuated total reflectance infrared (ATR-IR) spectroscopy and taking advantage of the intense IR-active vibrational bands created when dopants such as iodine accept charge from a semiconducting polymer to generate polaronic species. The diffusion and permeability coefficients for iodine within poly(3-hexylthiophene) (P3HT) are determined to be $2.5 \times 10^{-11} \pm 1.2 \times 10^{-11}$ cm^2/s and $2.4 \times 10^{-8} \pm 1.2 \times 10^{-8}$ cm^2/s·atm, respectively. The approach is applied to P3HT/PCBM (1:1 mass ratio) films, and the diffusion and permeability coefficients through these composite films are determined to be $7.8 \times 10^{-11} \pm 2.8 \times 10^{-11}$ cm^2/s and $4.8 \times 10^{-8} \pm 1.3 \times 10^{-8}$ cm^2/s·atm, respectively. Finally, the approach is extended to determining iodine diffusion within the polycrystalline semiconductor tetraphenylporphyrin (TPP) in a bilayer film with P3HT, and the diffusion coefficient of iodine through TPP is determined to be $7.1 \times 10^{-14} \pm 1.1 \times 10^{-14}$ cm^2/s. Although the current paper determines diffusion and permeability for the dopant iodine, this approach should be applicable to a wide array of dopants and polymeric and small-molecule semiconductors of interest in photovoltaic and electronic applications.

KEYWORDS: organic photovoltaics, dopants, diffusion, P3HT
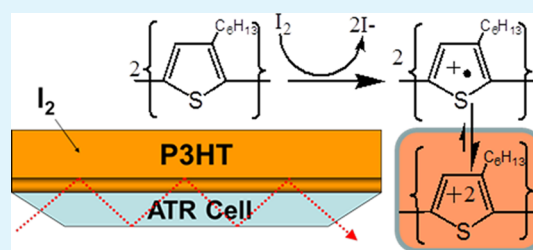
■ INTRODUCTION

Organic and polymeric semiconductors have been the subject of intense inquiry in recent years, especially with regard to their relevance to the development of organic photovoltaic cells.[1−5] In recent years, chemical doping has been explored as an approach to tailor and enhance the properties of organic and polymeric semiconductors.[6−10] Hole doping of organic semiconductors can be performed using a variety of species such as bromine, iodine, or organic molecules such as tetrafluorotetracyanoquinodimethane (F$_4$-TCNQ).[6,11] Electron doping has been performed with metals, such as lithium or cesium, and organometallics.[6−8] Molecular precursors have also been used, which upon thermal annealing dope their host films.[9,10] In analogy to complementary metal−oxide semiconductor electronics, the development of controlled doping processes for organic electronics is anticipated to provide a major breakthrough in terms of realizing useful devices.[6,10] Chemical doping of organic semiconductors can control the charge carrier density within devices, reduce contact resistance at interfaces, and increase mobility through trap filling.[6,8,10,11] Controlled doping is especially important in p−n and p−i−n devices.[12] Organic light-emitting devices (OLEDs) and OPVs have shown enhanced performance as a result of chemical doping.[6,13] In the case of OPVs, a 50% enhancement in efficiency has been reported as a result of iodine doping of poly(3-hexylthiophene) (P3HT)/PCBM devices.[13] Small-molecule dopants such as iodine and alkali metals have been reported to lack diffusional stability.[6,8,12,14] In order to achieve doping with diffusional stability, larger organic molecules such as tetracyanoquinodimethane (TCNQ) and F$_4$-TCNQ have been utilized.[6] However, there are very few reports for the diffusion parameters of dopants within organic semiconductors.[15,16] It would be valuable to understand the diffusional properties of dopants within organic semiconductors to determine how fabrication, processing, annealing, and operating conditions impact the dopant distribution.

To the best of our knowledge, the diffusion constant of iodine through P3HT films has yet to be reported. Diffusion of gases through polymeric films is routinely measured, most often through differential pressure experiments.[17,18] The diffusion coefficient for oxygen through P3HT films was obtained on free-standing films by measurement of the oxygen partial pressure differences across the film over time.[15] Iodine diffusion in polymers such as polycarbonate (PC), poly(ethylene terephthalate) (PET), and acrylonitrile−butadiene−styrene (ABS) has been measured using positron annihilation lifetime techniques.[19] The diffusion of iodine in polycrystalline porphyrin films has been measured electrochemically in

Schottky barrier devices.[16] However, simpler approaches to measuring the diffusional properties of dopants within organic and polymeric semiconductors will be valuable, especially as the importance of these materials grows and also the importance of understanding and controlling doping processes within these materials grows.

In the present work, we measure iodine diffusion within regioregular P3HT at a low concentration of iodine dopant. This approach takes advantage of the intense IR-active vibrational (IRAV) modes present in P3HT when it is doped by iodine. These IRAV modes result from the polaronic or bipolaric species generated upon charge transfer from P3HT to iodine.[20] These intense bands (present as a broad absorption at ~2500−4000 cm^{-1} as well as structured absorptions at 900−1300 cm^{-1}) are present in most conducting polymers (i.e., polyacetylene and related polymers) and are particularly intense in P3HT.[20,21]

In our experiment, the iodine dopant is delivered in the gas phase to the film. The film is deposited on an attenuated total reflectance infrared (ATR-IR) cell, and the rate of diffusion of the analyte through the film is observed through the growth of IRAV bands over time (see Figure 1) By plotting the intensity
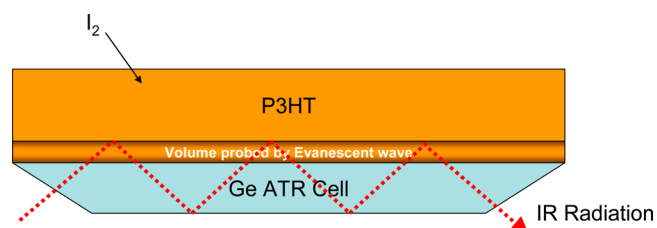

Figure 1. Scheme for the use of ATR-IR spectroscopy to detect dopant diffusion. ATR-IR uses evanescent wave interaction to probe a thin layer at the interface of P3HT and the germanium ATR cell. The depth of penetration is determined by the wavelength and incidence angle (see the text for details). The diffusion of iodine through P3HT can be determined because iodine dopes nearby P3HT, creating a polaron with intense IR absorption.
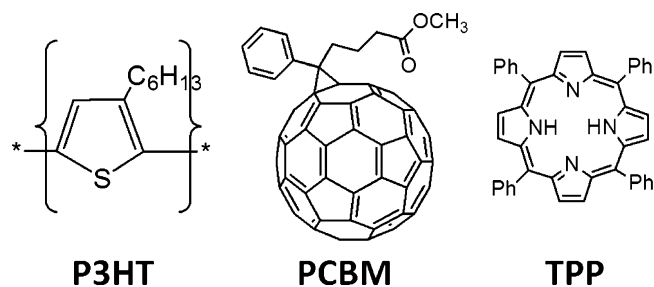

Figure 2. Molecules studied: regioregular P3HT, PCBM, and TPP.

of these bands over time, we can measure indirectly the rate of diffusion of iodine through P3HT through the growth of these bands. (The doping of P3HT is considered fast and is observed to be reversible.) Iodine diffusion through P3HT could occur as an I_2 molecule. Diffusion could also be envisioned to occur as an ion (I^- or I_3^-) moving together with the polaron through the film. Most likely, a combination of these mechanisms is involved; however, the exact molecular mechanism of diffusion is beyond the scope of this initial study. Using the time-lag approach, we can calculate the diffusion coefficients for iodine through P3HT.[15,17] The slope of the IRAV intensity curves versus time was used to calculate P3HT permeability to iodine.

Using this approach, we have also measured the diffusion of iodine through a composite film composed of P3HT/PCBM (1:1 mass ratio), which is the prototypical bulk heterojunction composition for organic photovoltaics. We have determined the diffusion and permeability coefficients for iodine within this composite film.

The ATR-IR method of measuring iodine diffusion can be extended to general organic and polymeric semiconducting films. We have measured the diffusion of iodine through a polycrystalline small-molecule organic semiconductor film using a bilayer approach. In this experiment, we first deposit a thin P3HT film (approximately 0.5 μm), followed by evaporation of a thin film of the organic semiconductor tetraphenylporphryin (TPP; chosen because diffusion of iodine through this film has been reported previously).[16] In this experiment, iodine diffusion through the TPP film is observed by intense IRAV absorption, which appears as soon as the dopant reaches the P3HT film. Using this bilayer approach, our method for measuring diffusion can be applied broadly to any material that can be deposited on top of our P3HT film.

Although all experiments in this manuscript are performed for iodine, our approach can be generalized to other dopants and, with appropriate modifications, should be applicable to measuring the diffusion of technologically important dopants such as TCNQ and F$_4$-TCNQ. The diffusion and permeability constants for iodine through P3HT will be of value in the design of gradient-doped P3HT systems with applications in OPV, OLED, and organic electronics.[6] It will also serve as a model for diffusion of other species within P3HT, which may be relevant for understanding of OPV stability and photo-degradation.[22,23]

■ EXPERIMENTAL SECTION

Materials. Iodine, regioregular P3HT (number-average molecular weight M_n; 15−45 K), TPP, and chlorobenzene were obtained from Sigma Aldrich and used as received. PCBM was purchased from Nano-C. ATR measurements were made using a Nicolet Magna 560 IR spectrometer with a multibounce germanium ATR cell (trough). Film thickness measurements were performed using a Wycko optical profilometer.

Sample Preparation. *P3HT Films.* P3HT (approximated 20−25 mg) is dissolved in 1.2 mL of chlorobenzene. This solution is heated to 40 °C to aid dissolution of P3HT. The solution is filtered through a 1 μm syringe filter and deposited onto the germanium ATR cell. The ATR cell is slowly (~0.2 cycles/s) rotated using a spin coater, in order to ensure an even film. Solvent evaporation takes approximately 2 h. The resultant film (1.8−3 μm) is annealed under a nitrogen atmosphere in a vacuum oven for 30 min at 100 °C. The resulting film is subjected to iodine exposure within a glass enclosure that is seated upon the ATR cell within the IR spectrometer.

P3HT/PCBM Films. A total of 12.5 mg of P3HT and 12.5 mg of PCBM are dissolved in 0.8 mL of chlorobenzene with slight heating (40 °C). The resulting solution is filtered through 1 μm syringe filter and deposited onto the germanium ATR cell. The films are annealed, and iodine diffusion is measured in a manner analogous to P3HT films (vide supra).

TPP/P3HT Bilayer Films. P3HT (14 mg) is dissolved in 0.8 mL of chlorobenzene at 40 °C. Approximately 0.08 mL of this solution is deposited onto the germanium ATR cell to generate a thin film (~500 nm; annealed as described above). TPP is deposited on top of the P3HT film by thermal evaporation using an Edwards Auto 306 thermal evaporator (base pressure 5 × 10^{-6} Torr; rate 0.5 Å/s).

ATR-IR Spectroscopy. The P3HT film on the germanium ATR cell is placed within the IR spectrometer. A homemade glass enclosure is place on top of the cell. I_2 is heated to 50 °C in a vial under N$_2$ and placed under the glass enclosure. Measurements of IR spectra are

8301

dx.doi.org/10.1021/am401799k | ACS Appl. Mater. Interfaces 2013, 5, 8300−8307

taken immediately after iodine exposure and at intervals for a period of approximately 2000−4000 s. All diffusion experiments are performed at room temperature.

For experiments with P3HT and P3HT/PCBM, a normal curve is made to determine the amount of I_2 introduced to the film (see Figure 5). Quantitative solutions of I_2 in chlorobenzene are made. P3HT is dissolved in a separate chlorobenzene solution. The P3HT and I_2/chlorobenzene solutions are mixed in ratios to create the appropriate concentrations (measured as I_2/P3HT w/v). These films are deposited without filtering because I_2/P3HT precipitates to varying extents depending on the iodine concentration presumably because of the lower solubility of the charge-transfer complex of I_2 and P3HT. The I_2/P3HT films are permitted to dry under ambient conditions. Thicknesses (~5 μm) are obtained that are much thicker than the pentration depth of ~500 nm for ATR measurement. A normal curve is generated for P3HT/PCBM using the same procedure.

■ RESULTS

Figure 1 illustrates the ATR-IR spectra for P3HT films deposited on germanium that has been exposed to iodine vapor. The spectrum for pristine P3HT is the black spectrum in Figure 1. In addition to the peaks in the CH stretch region (2800−3000 cm^{-1}), there are three characteristic peaks at 1350−1510 cm^{-1} and another characteristic band at 819 cm^{-1}. Assignments for P3HT IR spectra have been published.[24] The peak at 1510 cm^{-1} has been assigned to the asymmetric C═C ring stretch. The peak at 1456 cm^{-1} is assigned to the symmetric C═C ring stretch. The peak at 1378 cm^{-1} is assigned to the deformation/vibration of terminal methyl in the hexyl side chain. The absorption at 819 cm^{-1} is assigned to the out-of-plane distortion of C−H on the ring.[25]

Upon introduction of iodine vapor to the sample, an increase in the IRAV mode intensity over time is plotted. Several bands are observed in the IR spectra including a broad absorption between 1500 and 4000 cm^{-1} and several strong IRAV bands between 1000 and 1500 cm^{-1} associated with the polaronic charge carrier.[20,21] These polaronic bands are induced by iodine present within the film as a result of electron transfer from the P3HT film to iodine. This process is facile and reversible.[20,21] Because the iodine concentration is linearly related to the strength of the polaronic band (see Figure 3), the polaronic IRAVs can be used to quantify the iodine diffusion rates within the P3HT films. Because there is a broad increase in the IR spectra as a result of the iodine dopant, we can monitor the diffusion at several wavelengths and have independent measurements to calculate the diffusion constant. As can be seen in Figure 3, we have calculated diffusion using absorption values averaged between 1280 and 1340 cm^{-1}, 3100 and 3200 cm^{-1}, and 3900 and 4000 cm^{-1} because these windows capture the broad hump of the polaronic absorption as well as the narrow feature of the absorption. The further advantage of this approach is that the penetration depth for the ATR measurement is dependent on the wavelength, and the measurement performed at 3900−4000 cm^{-1} penetrates a shorter distance into the P3HT film than the measurement at 1280 cm^{-1}, as defined by eq 1.[26]

$$dp \ (\text{depth of penetration}) = \frac{\frac{\lambda}{n_1}}{2\pi\left[\sin^2\theta - \left(\frac{n_s}{n_1}\right)^2\right]^{1/2}} \tag{1}$$

The refractive indices n_1 and n_s are the refractive indices for germanium ($n_1 = 4$) and P3HT ($n_s = 1.7$), respectively. The refractive index at IR wavelengths is obtained by extrapolation
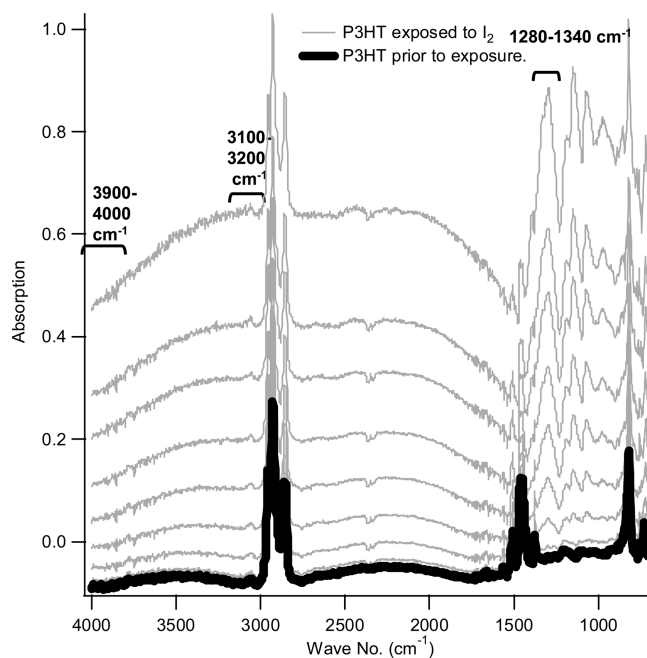

Figure 3. IRAV bands in P3HT activated upon iodine exposure. The black spectrum is the ATR-IR spectrum of the P3HT film prior to iodine exposure. The gray curves are spectra of P3HT after various times of iodine exposure. Times range from 0 to 2870 s. Data for kinetic analysis of iodine diffusion within the P3HT film are taken at 1280−1340, 3100−3200, and 3900−4000 cm^{-1}.

from published values of n_s for P3HT in the visible to near-IR.[27] The angle $\theta = 45°$ and is the incidence angle for the ATR cell.

For 3900 cm^{-1}, the depth of penetration is approximately 180 nm, whereas for 3100 cm^{-1}, it is 224 nm, and for 1280 cm^{-1}, it is 537 nm. This difference in penetration depth for the ATR cell results in a different effective thickness, which is experimentally observed in Figures 3 and 4 as a difference in the time lag before a steady-state increase in the iodine concentration is observed versus time.

The average absorption over the bands specified above was plotted versus time for each sample measured, and a representative sample is presented in Figure 4. The overall profile of absorption increase versus time is presented in the inset, and the main figure highlights the linear portion of the increase and the time lag before this linear increase. The time lag, or x-intercept value, is used to calculate the diffusion coefficient for iodine through the P3HT sample, and these values are presented in Table 1. Equation 2 is used to relate the time lag to the diffusion constant.[15,17]

$$\theta = \frac{l^2}{6D} \tag{2}$$

The value of l is determined to be the film thickness measured using optical profilometry with the penetration depth subtracted. Using this approach, we can calculate the diffusion constant for iodine at different wavelengths (with corresponding penetration depths). By utilizing multiple penetration depths, we can be more confident that we are measuring iodine diffusion through the film and not other processes such as iodine absorption or polaron movement.[20]

In order to determine the permeability from our IR data in Figure 3, the relationship between the absorption data and
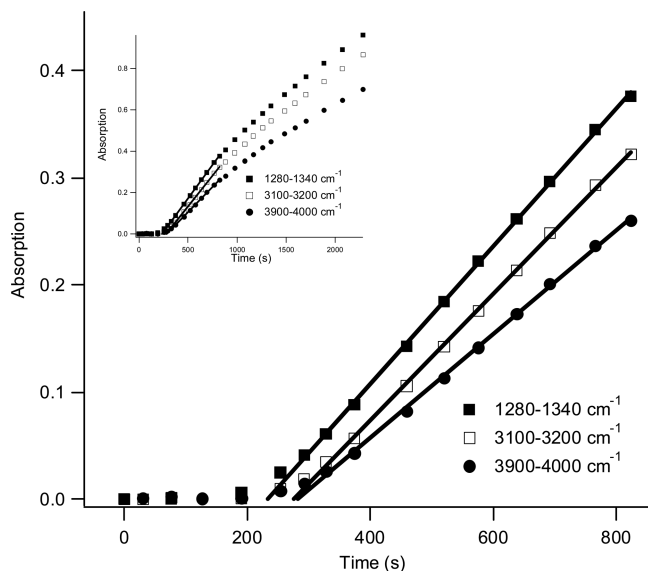
Figure 4. Monitoring the increase in IRAV band absorption versus time for P3HT upon exposure to iodine. Absorption monitored at 1280−1340, 3100−3200, and 3900−4000 cm^{-1}. Linear portion of growth fit to determine the x intercept to calculate the diffusion constant within iodine. The inset shows the entire time span investigated, showing saturation of absorption at long exposure times.
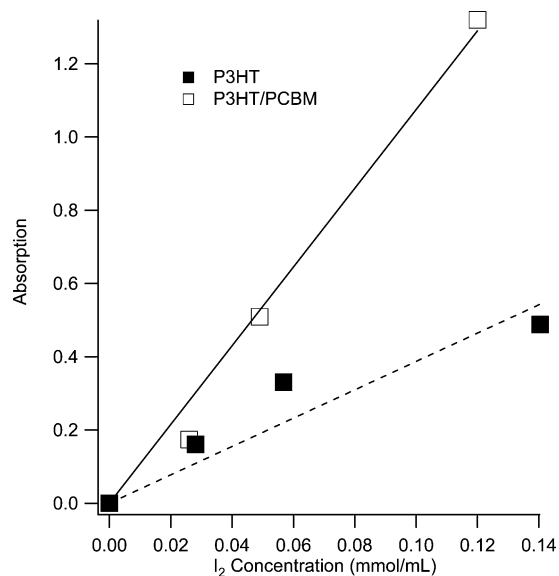

Figure 5. Calibration of iodine response. Measurement of the IRAV intensity in ATR-IR spectra induced by specific concentrations of iodine in P3HT and P3HT/PCBM films. Average absorption of 1280−1340 cm^{-1} for P3HT. Average absorption of 1300−1325 cm^{-1} for 1:1 P3HT/PCBM.

iodine concentration needs to be known. We have done this by depositing films of P3HT/I$_2$ solutions in which the iodine concentration is known. These films exhibit the same IRAV absorptions as those seen in P3HT doped with iodine vapor, and the relationship between the iodine concentration and absorption is linear. The data for absorption at 1280 cm^{-1} are presented in Figure 5. Although this is not an extinction coefficient for iodine or for the polaron, it can be used as an effective extinction coefficient for iodine in our vapor-doping experiments because the iodine concentration in the film is linearly related to IRAV absorption. Because we are performing an ATR experiment, the path length and penetration depth are dependent on the wavelength chosen, and so the data presented in Figure 5 are only applicable to 1280 cm^{-1}.

We used the coefficient of 11.317 (mmol/mL)$^{-1}$ to convert data in Figure 3 into the concentration versus time data presented in Figure 6. These data were used to determine the permeability of the P3HT film to iodine. Figure 6 is representative of the multiple samples tested and tabulated in Table 1. The slope in Figure 4 ($d[M]/dt$) is used to calculate the permeability using eq 3, which is derived for permeability calculations in gas diffusion experiments, and dp/dt is the pressure differential.[17]

$$ P = \frac{dp}{dt}\left(\frac{Vl}{pA}\right)\left(\frac{273}{T}\right) \tag{3} $$

Figure 6. Iodine concentration within the P3HT film probed by ATR-IR experiment at 1280−1340 cm^{-1}. The slope is related to the permeability of iodine within P3HT.

Our experimental quantity $d[M]/dt$ can be related to dp/dt, as illustrated in eq 4

Table 1. Diffusion, Permeability, and Solubility Coefficients for Iodine in P3HT

data set	$D_{I_2\text{-P3HT}}$ (cm^2/s)	film thickness (cm)	penetration depth (cm)	P (cm^2/s·atm)	S (cm^3/cm^3·atm)
1	3.90×10^{-11}	2.3×10^{-4}	5.37×10^{-5}	3.80×10^{-8}	975
2	1.75×10^{-11}	3.0×10^{-4}	5.37×10^{-5}	1.63×10^{-8}	932
3	1.83×10^{-11}	1.8×10^{-4}	5.37×10^{-5}	1.82×10^{-8}	992
average	$2.5 \times 10^{-11} \pm 1.2 \times 10^{-11}$			$2.42 \times 10^{-8} \pm 1.2 \times 10^{-8}$	966 ± 31

Table 2. Iodine Diffusion, Permeability, and Solubility Coefficients through the P3HT/PCBM Composite Film (1:1 by Mass)

data set	$D_{I_2\text{-}P3HT}$ (cm^2/s)	film thickness (cm)	penetration depth (cm)	P (cm^2/s·atm)	S (cm^3/cm^3·atm)
1	5.5×10^{-11}	3.2×10^{-04}	5.37×10^{-5}	4.15×10^{-8}	754
2	1.1×10^{-10}	4.0×10^{-04}	5.37×10^{-5}	7.09×10^{-8}	644
3	7.0×10^{-11}	4.0×10^{-04}	5.37×10^{-5}	5.71×10^{-8}	816
Average	$7.8 \times 10^{-11} \pm 2.8 \times 10^{-11}$			$5.65 \times 10^{-8} \pm 1.5 \times 10^{-8}$	738 ± 87

$$\frac{dp}{dt} = \frac{dn}{dt}\left(\frac{RT}{V}\right) = \frac{d[M]}{dt}(Adp)RT \qquad (4)$$

$$P = \frac{d[M]}{dt}\left(\frac{273Rldp}{p}\right) \qquad (5)$$

where dn/dt = flux of molecules (units: mol/s), which is related to the slope obtained from Figure 4, which is the flux (units: mols/L·s) multiplied by the volume being probed by the ATR experiment (area × depth of penetration = Adp). Using these relationships (eqs 3−5), we can obtain values for the permeability, which are presented in Table 1.

Finally because the permeability and diffusion coefficient are related by the solubility parameter, we can calculate this parameter S using eq 6.[17]

$$S = P/D \qquad (6)$$

Results for P3HT/PCBM. P3HT/PCBM (1:1 by mass) was dissolved in chlorobenzene and deposited as a film onto the germanium ATR cell. Film thicknesses ranged from 3 to 4 μm (see Table 2). The IR spectra for the P3HT/PCBM film before doping and later into doping are presented in Figure 7. The
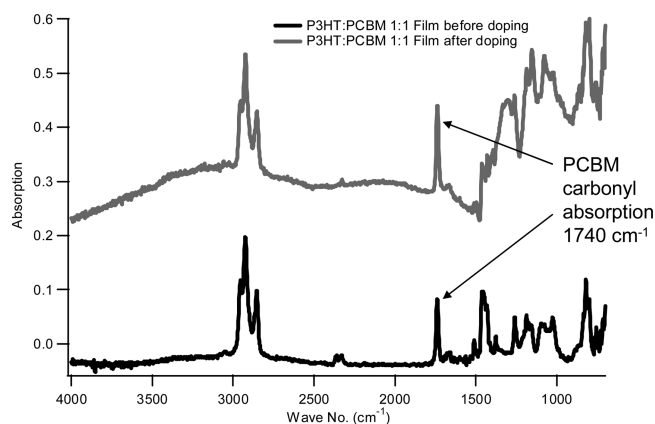
Figure 7. ATR-IR spectra for P3HT/PCBM films deposited on a germanium substrate before and after iodine doping.

main feature of PCBM is the carbonyl absorption observed at 1740 cm^{-1}.[25] The polaronic absorption appears more or less the same in the composite as in neat P3HT films with a broad absorption band from 2000 to 4000 cm^{-1} and narrower features in the 800−1400 cm^{-1} range, with a notable band at 1280−1340 cm^{-1}. An absorption from PCBM at 1260 cm^{-1} overlaps with the polaronic absorption. For this reason, a narrower window of 1300−1325 cm^{-1} is used to probe diffusion (see Figure 8).

The time lag approach was used to calculate diffusion coefficients, permeability, and solubility parameters for P3HT/PCBM films. A normal curve for the 1:1 P3HT/PCBM film was made in a manner analogous to neat P3HT films (see Figure 5). The iodine concentration is related to polaronic
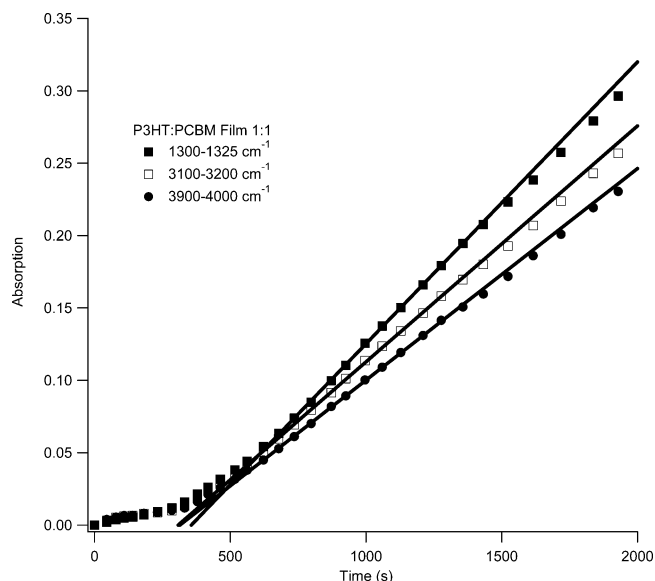
Figure 8. Monitoring the increase in IRAV band absorption versus time for P3HT/PCBM (1:1) films upon exposure to iodine. Absorption monitored at 1300−1325, 3100−3200, and 3900−4000 cm^{-1}. Linear portion of growth fit to determine the x intercept to calculate the diffusion constant within iodine.

absorption through the extinction coefficient of 3.87 (mmol/L)$^{-1}$, which is slightly less than half of the extinction coefficient for neat P3HT, as expected because P3HT is diluted because of the presence of PCBM. Using this value, we can calculate the concentration of iodine that arrives at the penetration depth for 1300−1325 cm^{-1} and use this to determine the permeability and solubility parameters, as specified previously for neat P3HT (see Table 2).

Measuring Diffusion through TPP. An adaption of the time-lag approach is used to measure diffusion of iodine through the polycrystalline thin film TPP. For these experiments, a thin layer (~500 nm of P3HT is deposited onto the germanium ATR cell, followed by thermal evaporation of TPP). The ATR-IR spectra for TPP and the P3HT/TPP bilayer are presented in Figure 9. The depth of penetration at 1300 cm^{-1} is approximately 500 nm, and for this reason, P3HT absorption dominates the ATR-IR spectra for the bilayer. (At higher wavelengths, the depth of penetration is even less.) Furthermore, as a control, a 150 nm TPP thin film evaporated directly onto the germanium ATR cell and was subjected to iodine exposure, and no significant changes are observed in the IR spectrum on the time scale of our doping experiments. Exposure of the bilayer to iodine does result in an absorption change consistent with the P3HT polaron (see Figure 9). Representative data are presented in Figure 10. An initial linear slope is observed from the onset of iodine exposure. We observe further increases in the polaronic signal superimposed on this linear signal. The immediate onset of the linear signal suggests to us rapid diffusion through defects, grain boundaries,
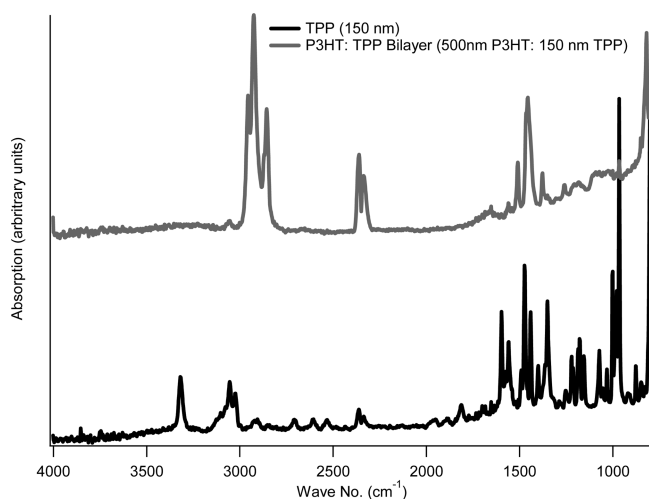
Figure 9. IR spectra for TPP (150 nm) and a P3HT (500 nm)/TPP (150 nm) bilayer deposited on ATR cell. The bilayer spectra are dominated by the P3HT signal because the depth of penetration for the germanium cell ranges from 180 to 537 nm across the wavelength range.
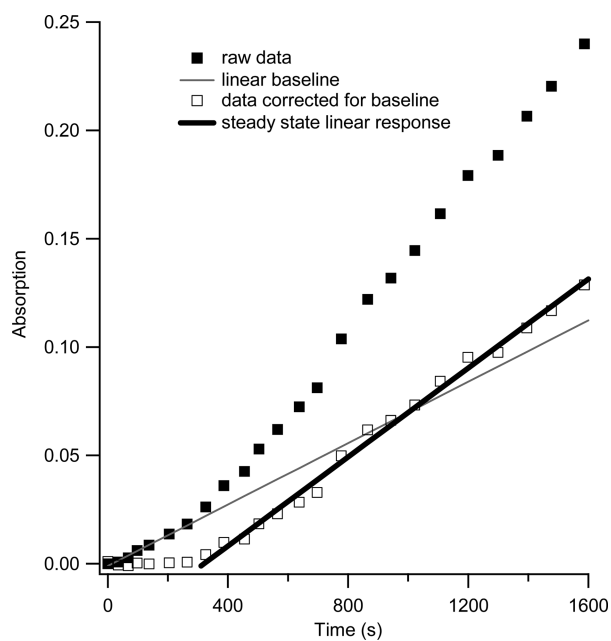

Figure 10. Measuring the diffusion of iodine through a polycrystalline TPP thin film deposited on top (0.5 μm P3HT film). Iodine diffusion observed via an increase in IRAV mode absorption in P3HT (filled squares: raw data). Defects and grain boundaries in the thin film result in immediate linear response upon exposure to iodine. Absorption resulting from diffusion through TPP superimposed on this linear background signal. The linear background subtracted out yields corrected data (open squares). A fit to the linear growth of this curve yields diffusion parameters for iodine through TPP.

imperfections, and pin holes within the 100−150 nm TPP film. Iodine diffusion through these defects would be very fast, and near-immediate interaction with the underlying P3HT film would register as a polaronic absorption because the P3HT thickness is smaller than the penetration depth. This linear response can be subtracted out (see Figure 10) to reveal the absorption profile, which results from diffusion through the polycrystalline TPP film. Application of the time-lag approach

to this data allows calculation of the diffusion constant for iodine through TPP. Measurement was performed for films of three different thicknesses, and the diffusion coefficients determined by this approach were $7.1 \times 10^{-14} \pm 1.1 \times 10^{-14}$ cm^2/s.

■ DISCUSSION

Film deposition of regioregular P3HT (Aldrich; 15−45 K) was performed from a chlorobenzene solvent, via dropcasting. The films once deposited were annealed at 100 °C under a nitrogen atmosphere for 30 min. Deposition and annealing were performed in an attempt to standardize the resultant film and conform these film properties to those typically obtained.[28,29] Annealing is expected to increase the crystallinity within the P3HT film.[29] Although annealing was performed under a nitrogen atmosphere, film deposition was performed in an ambient atmosphere, and the humidity was not controlled. Furthermore, it is well-known that P3HT film morphologies are typically far from equilibrium,[28] so small changes in the process temperature or history could result in variations in the measured parameters obtained between different samples reported in Table 1.

Diffusion, permeability, and solubility coefficients were obtained using the time-lag approach.[15,17,18] In this approach, the x intercept of the linear portion of the curve is used to calculate the diffusion coefficient using eq 2. The slope of the linear portion of the curve is used to calculate the permeability using eq 5. As can be seen in the inset for Figure 2, the absorption signal for the polaron saturates over time. In Figure 2, deviation from linearity occurs at an optical density of 0.6 (corresponding to an iodine loading of approximately 0.06 mmol/mL). These deviations from linearity could result from possible repulsive interactions of P3HT polarons at higher density. The reduced mobility has been reported for P3HT samples under exposure to high oxygen pressures (4−10 atm), where increased carrier concentration may have similar effects.[15]

Oxygen diffusion constants have been measured for P3HT and determined to be 1.2×10^{-8} cm^2/s.[15] These values were determined by measuring the pressure of oxygen diffusing through a thick P3HT film. The low diffusion rate was considered to be, in part, due to the semicrystalline nature of P3HT, which is believed to retard diffusion. Our iodine diffusion constants are measured to be ~500× slower than those for oxygen, and this difference is consistent with the size difference between I$_2$ and O$_2$ (the kinetic radius for O$_2$ is 3.45 Å, whereas I$_2$ has a kinetic radius of 6.5 Å).[30,31]

Iodine diffusion has been measured in PET, ABS, and PC using the positron anniliation lifetime technique.[19] Non-Fickian diffusion was observed in ABS and PET, but Fickian diffusion was observed for PC. Diffusion coefficients for the Fickian component of diffusion in ABS and PET were found to be 1.55 and 1.59×10^{-8} cm^2/s, and in PC, a diffusion coefficient of 5.7×10^{-9} cm^2/s is reported. In the case of crystalline solids (MTPP, where M = Mg, Cu, Zn, H$_2$, and Ni), diffusion coefficients ranging from 1.1 to 8.2×10^{-15} have been reported.[16] Compared to these reported values, our measured diffusion coefficient for iodine within P3HT appears to be reasonable (2.5×10^{-11} cm^2/s) because P3HT is a semicrystalline polymer that has properties intermediate between those of the crystalline porphyrins (~10^{-15} cm^2/s) and thermoplastic polymers (10^{-8}−10^{-9} cm^2/s).

Although all films were handled and processed using the same procedure, there is some variability in the measured values for diffusion. A comparison of data set 1 with 2 and 3 shows a deviation in the measured diffusion coefficient (see Table 1). Because this deviation is also observed in the permeability (see below) and because the solubility parameter obtained (S) is relatively constant (see Table 1) for all measurements, we do not think the difference in the measured mobility is a random error but rather is due to the subtle difference in morphology and processing history as discussed above, which could result from the fact that these P3HT films are deposited and annealed far from equilibrium.[28]

In contrast to reports on the permeability of oxygen within P3HT,[15] the permeability of iodine that we measure is much higher (2.4×10^{-8} vs 3.4×10^{-11} cm^2/s·atm). The interaction of iodine appears to be much stronger with P3HT than the interaction of oxygen, and this is consistent with the large solubility parameter of iodine within P3HT. Oxygen has a solubility parameter reported to be 0.2, which is several orders of magnitude lower than that of iodine.[15] However, oxygen is also reported to only form very weak complexes with P3HT[15] and, in its ground state, is not efficient in doping P3HT.[20] The relationship between the permeability and diffusion is inverted for iodine and oxygen within P3HT. Iodine diffusion is slow because of its large size, but the iodine permeability is large because of the strong interaction of I_2 and P3HT, which is further evidenced by the high solubility parameter. In comparing iodine permeability within P3HT, we can consider permeabilities for other small molecules through polymers. Values for the permeability of methane within natural and synthetic rubbers range from 0.6 to 12.5×10^{-8} cm^2/s·atm. Methane has a kinetic radius that is slightly smaller than that of iodine (4 as opposed to 6.8), but the permeability values are in roughly the same range.[17] It was somewhat surprising to obtain a very high value of the solubility coefficient (966 ± 31 cm^3/cm^3·atm). In all of the samples tested, we obtained a very consistent value for S, as calculated from eq 6, which suggests that although some variability in the diffusion and permeability are present in the different P3HT films, the ratio of these as determined by the solubility parameter is fairly constant for these different P3HT films. The very high value is similar to the solubility coefficients for water within hydrophilic polymers such as water in poly(ethyl methacrylate) ($S = 236$ cm^3/cm^3·atm), cellulose nitrate ($S = 1824$ cm^3/cm^3·atm), and Kapton ($S = 2168$ cm^3/cm^3·atm).[32] The large solubility coefficient calculated from our data is consistent with iodine doping studies on other organic semiconductors such as pentacene in which very high ratios of I_2/pentacene (6:1) are achievable by exposure of pentacene to iodine vapor.[33] P3HT is similar to pentacene as a conjugated π system, and this π system appears to have a great affinity for iodine via charge-transfer interactions.

When we measured diffusion in P3HT/PCBM composites, we observed a roughly 3-fold increase in diffusion within the composite as opposed to that of neat P3HT (7.8 vs 2.5×10^{-11} cm^2/s). P3HT/PCBM composites are believed to be composed of neat P3HT domains, P3HT/PCBM mixed domains, and also small PCBM domains.[34,35] The results suggest that dopant diffusion through the mixed domain is faster, possibly because of a reduced crystallinity in these regions and a greater free volume. The solubility parameter for the composite is slightly lower than for neat P3HT, which suggests that I_2 is less soluble within PCBM than P3HT. Because the permeability is the

product of the solubility parameter and diffusion coefficient, the values for P3HT/PCBM turn out to be lower than those for neat P3HT. The increased diffusion in the composite film and the reduced solubility in the PCBM domain suggest that diffusion is occurring primarily through the P3HT phases. This diffusion is occurring faster as a result of the greater disorder and likely greater free volume in the P3HT phases of the composite.

In order to generalize our method to address diffusion measurements within a general organic or polymeric semiconductor, we developed a bilayer approach. In this approach, we deposit a thin P3HT layer onto our germanium ATR cell, which will serve as a reporter for iodine diffusion. The thickness of this film ($\sim$500 nm) is chosen such that it is less than the penetration depth probed by the ATR-IR method. At 1300 cm^{-1}, this penetration depth is 537 nm. As a test molecule we have chosen TPP because iodine diffusion through this semicrystalline polymer has been reported (5.2×10^{-15} cm^2/s).[16] TPP is deposited using thermal evaporation, and films of 100−150 nm are deposited to make the diffusion times tractable. TPP itself does not show any observable IRAV modes as a result of iodine exposure, and as such, the appearance of the IRAV is an indicator of iodine diffusion through the TPP film to the underlying P3HT film (see Figure 10). We observed with these thin semiconductor films that P3HT IRAV absorption increases immediately upon exposure to iodine vapor, and the initial response is linear. At later times, we see an acceleration in the absorption increase. We interpret the initial linear response as being due to rapid diffusion of iodine through defects and grain boundaries in the thin TPP films. This fast diffusion, which is several orders of magnitude faster than diffusion through the TPP crystal itself, manifests in the linear response. If we subtract this initial linear response, we recover a IRAV absorption increase, which represents diffusion through the crystal itself. The time-lag method can be applied to these data to determine the time-lag Θ for iodine diffusion through the TPP crystal. These data are presented in Table 3.

Table 3. Diffusion of Iodine through TPP: Summary of the Results

sample	Θ (s)	TPP thickness (nm)	diffusion coefficient (cm^2/s)
1	276	100	6.0×10^{-14}
2	320	125	8.2×10^{-14}
3	520	150	7.2×10^{-14}
average			$7.1 \times 10^{-14} \pm 1.1 \times 10^{-14}$

Three experiments were performed and provided consistent data for diffusion through TPP obtained at three different film thicknesses (100, 125, and 150 nm). The value we obtained using our methods is $7.1 \times 10^{-14} \pm 1.1 \times 10^{-14}$ cm^2/s. The value we obtained is roughly 1 order of magnitude larger than the value of 5.2×10^{-15} cm^2/s reported previously by Nevin.[16] In Nevin's approach, the conductivity of a porphyrin film is measured, and a model is used to relate this to the dopant (iodine concentration). The conductivity profile over time is used to determine the diffusion constant of iodine within the porphyrin film. Measurements were made at 20 °C compared to our measurements at 25 °C. Film deposition in our samples was performed at 0.5 Å/s, whereas deposition in Nevin's work occurred at a much faster rate (6 Å/s), which could result in differences in film morphology. Considering these differences in the measurement methods, temperature, and film deposition

conditions, some differences in the measured diffusion coefficients can be expected. However, the values that we obtain are reasonable, and the reproducibility of our measurements provides confidence in our approach.

CONCLUSION

In summary, the intense IRAV bands of the P3HT polaron provide a very sensitive probe for diffusion of dopants within P3HT when coupled with ATR-IR spectroscopy. We have demonstrated the use of these IRAV absorptions to determine the diffusion, permeability, and solubility coefficient of iodine within P3HT and P3HT/PCBM composite films. We have generalized this approach to determine the diffusion of iodine through a polycrystalline TPP thin film, demonstrating that the approach can be applied to almost any small molecule or polymeric film deposited on P3HT. Most semiconducting polymers exhibit IRAV modes when doped, as a result of mobile polaronic species, and as such, many could be studied using this technique.[20] Diffusion of other dopants and impurity molecules could also be studied using this approach. Of special interest would be the application of this approach to study the diffusion of larger molecular dopants such as TCNQ or F$_4$-TCNQ. Although at room temperature diffusion of these dopants may be relatively slow within a polymeric or crystalline semiconductor host, these materials may be subjected to diffusion at even slightly elevated temperatures. For example, it is well-known that the large fullerene PCBM is not diffusionally stable within P3HT films at elevated temperatures, and interdiffusion of PCBM is observable at temperatures as low as 50 °C.[36] Modifications of our approach utilizing a heated ATR cell and also adaption of the time-lag approach to measure diffusion from a bilayer containing a thin film of dopant and P3HT could be envisioned to address diffusion for this important class of dopant molecules. Because the approach is quite simple to implement using instrumentation available in most laboratories, it should find broad applicability in studies of dopant diffusion within these scientifically and technologically important materials.

AUTHOR INFORMATION

Corresponding Author
*E-mail: maliakal@lgsinnovations.com.

Notes
The authors declare no competing financial interest.

ACKNOWLEDGMENTS

REFERENCES

(1) Facchetti, A. *Chem. Mater.* **2011**, *23*, 733−758.
(2) Zhan, Z.; Zhu, D. *Polym. Chem.* **2010**, *1*, 409−419.
(3) Gledhill, S. E.; Scott, B.; Gregg, B. A. *J. Mater. Res.* **2005**, *20*, 3167−3179.
(4) Kippelen, B.; Bredas, J. L. *Energy Environ. Sci.* **2009**, *2*, 251−261.
(5) Myers, J. D.; Xue, J. G. *Polym. Rev.* **2012**, *52*, 1−37.
(6) Walzer, K.; Maennig, B.; Pfeiffer, M.; Leo, K. *Chem. Rev.* **2007**, *107*, 1233−1271.
(7) Guo, S.; Kim, S. B.; Mohapatra, S. K.; Qi, Y. B.; Sajoto, T.; Kahn, A.; Marder, S. R.; Barlow, S. *Adv. Mater.* **2012**, *24*, 699−703.
(8) Qi, Y. B.; Mohapatra, S. K.; Kim, S. B.; Barlow, S.; Marder, S. R.; Kahn, A. *Appl. Phys. Lett.* **2012**, *100*, 083305.
(9) Oh, J. H.; Wei, P.; Bao, Z. N. *Appl. Phys. Lett.* **2010**, *97*, 243305.
(10) Wei, P.; Oh, J. H.; Dong, G. F.; Bao, Z. N. *J. Am. Chem. Soc.* **2010**, *132*, 8852−8853.
(11) Maennig, B.; Pfeiffer, M.; Nollau, A.; Zhou, X.; Leo, K.; Simon, P. *Phys. Rev. B: Condens. Matter Mater. Phys.* **2001**, *64*, 195208.
(12) Menke, T.; Ray, D.; Meiss, J.; Leo, K.; Riede, M. *Appl. Phys. Lett.* **2012**, *100*, 093304.
(13) Zhuo, Z.; Zhang, F.; Wang, J.; Wang, J.; Xu, X.; Xu, Z.; Wang, Y.; Tang, W. *Solid-State Electron.* **2011**, *63*, 83−88.
(14) Lu, M.; Nicolai, H.; Wetzelaer, G.-J.; Blom, P. *Appl. Phys. Lett.* **2011**, *99*, 173302.
(15) Abdou, M.; Orfino, F.; Son, Y.; Holdcroft, S. *J. Am. Chem. Soc.* **1997**, *119*, 4518−4524.
(16) Nevin, W. A. *Anal. Chem.* **1991**, *63*, 2414−2417.
(17) Amerongen, G. J. V. *J. Appl. Phys.* **1946**, *17*, 972−985.
(18) Meares, P. *J. Am. Chem. Soc.* **1954**, *76*, 3415−3422.
(19) Ramani, R.; Ranganathaiah, C. *Polym. Int.* **2001**, *50*, 237−248.
(20) Heeger, A.; Kivelson, S.; Schrieffer, J.; Su, W.-P. *Rev. Mod. Phys.* **1988**, *60*, 781−850.
(21) Fichou, D.; Horowitz, G.; Xu, B.; Garnier, F. *Synth. Met.* **1990**, *39*, 243−259.
(22) Grossiord, N.; Kroon, J. M.; Andriessen, R.; Blom, P. W. M. *Org. Electron.* **2012**, *13*, 432−456.
(23) Jorgensen, M.; Norrman, K.; Gevorgyan, S. A.; Tromholt, T.; Andreasen, B.; Krebs, F. C. *Adv. Mater.* **2012**, *24*, 580−612.
(24) Wei, H.; Scudiero, L.; Eilers, H. *Appl. Surf. Sci.* **2011**, *255*, 8593−8597.
(25) Shrotriya, V.; Ouyang, J.; Tseng, R.; Li, G.; Yang, Y. *Chem. Phys. Lett.* **2005**, *411*, 138−143.
(26) *Foundation Series User's Manual*; Thermoelectron Corp.: Madison, WI, 2002; p 85.
(27) Gevaerts, V.; Koster, L.; Wienk, M.; Janssen, R. *ACS Appl. Mater. Interfaces* **2011**, *3*, 3252−3255.
(28) Ruderer, M. A.; Muller-Buschbaum, P. *Soft Matter* **2012**, *7*, 5482−5493.
(29) Salleo, A.; Kline, R. J.; DeLongchamp, D. M.; Chabinyc, M. L. *Adv. Mater.* **2010**, *22*, 3812−3838.
(30) Davis, M.; Montes, C.; Hathaway, P. E.; Arhancet, J.; Hasha, D.; Garces, J. *J. Am. Chem. Soc.* **1989**, *111*, 3919−3924.
(31) Cecil, E. Direct Monte Carlo Simulations of a Binary Gas Free-Jet Flow Over a Flat Plate. *27th International Symposium on Rarified Gas Dynamics*, Pacific Grove, CA, 2010; AIP Conference Proceedings: Pacific Grove, CA, 2010; pp 236−241.
(32) Pauly, S. In *Polymer Handbook*, 3rd ed.; Brandrup, J., Immergut, E., Eds.; Wiley-Interscience: New York, 1989; Vol. 6, pp 435−449.
(33) Brinkmann, M.; Videva, V.; Bieber, A.; Andre, J.; Turek, P.; Zuppiroli, L.; Bugnon, P.; Schaer, M.; Nuesch, F.; Humphry-Baker, R. *J. Phys. Chem. A* **2004**, *108*, 8170−8179.
(34) DeLongchamp, D. M.; Kline, R. J.; Fischer, D. A.; Richter, L. J.; Toney, M. F. *Adv. Mater.* **2011**, *23*, 319−337.
(35) DeLongchamp, D. M.; Kline, R. J.; Herzing, A. *Energy Environ. Sci.* **2012**, *5*, 5980−5993.
(36) Verploegen, E.; Mondal, R.; Bettinger, C. J.; Sok, S.; Toney, M. F.; Bao, Z. A. *Adv. Funct. Mater.* **2010**, *20*, 3519−3529.